Journal: Computers and Geotechnics

Paper: Numerical investigation of multi-directional site response based on KiK-net downhole array monitoring data

Authors: Bo HAN, Lidija ZDRAVKOVIC, Stavroula KONTOE, David M.G. TABORDA

Submission: 11th December 2016

Dr. Bo HAN*- Corresponding Author
Professor of the Qilu Youth Scholar Program
School of Civil Engineering
Shandong University
Jinan 250061, China
e-mail: bo.han@sdu.edu.cn

Formerly Imperial College London
Department of Civil and Environmental Engineering
London SW7 2AZ, UK
e-mail: bo.han@imperial.ac.uk

Prof. Lidija ZDRAVKOVIC
Professor of Computational Geomechanics
Department of Civil and Environmental Engineering
Imperial College London
London SW7 2AZ, UK
e-mail: l.zdravkovic@imperial.ac.uk

Dr. Stavroula KONTOE
Senior Lecturer
Department of Civil and Environmental Engineering
Imperial College London
London SW7 2AZ, UK
e-mail: stavroula.kontoe@imperial.ac.uk

Dr. David M.G. TABORDA
Lecturer
Department of Civil and Environmental Engineering
Imperial College London
London SW7 2AZ, UK
e-mail: d.taborda@imperial.ac.uk

Numerical investigation of multi-directional site response based on KiK-net downhole array monitoring data

Bo Han[1], Lidija Zdravković[2], Stavroula Kontoe[2], David M.G. Taborda[2]

1: School of Civil Engineering, Shandong University, Jinan 250061, China. Formerly Imperial College London

2: Department of Civil and Environmental Engineering, Imperial College London, London SW7 2AZ, United Kingdom

Abstract. The multi-directional site response of a well-documented downhole array in Japan is numerically investigated with three directional (3-D) dynamic hydro-mechanically (HM) coupled Finite Element (FE) analysis. The paper discusses the challenges that 3-D modelling poses in the calibration of a cyclic nonlinear model, giving particular emphasis on the independent simulation of the shear and volumetric deformation mechanisms. The employed FE model is validated by comparing the predicted site response against the recorded motions obtained from the KiK-net downhole array monitoring system in Japan. The results show that, by employing the appropriate numerical model, a good agreement can be achieved between the numerical results and the monitored acceleration response in all three directions simultaneously. Furthermore, the comparison with the recorded response highlights the significance of the independent modelling of the shear and volumetric deformation mechanisms to the improvement of the numerical predictions of multi-directional site response.

Key words: multi-directional site response, hydro-mechanical coupling, finite element analysis, acceleration array data

1 Introduction

Site response analysis is widely employed in engineering practice and research to assess how a ground profile modifies the incoming bedrock motion in terms of amplitude, frequency content and duration. In most cases one-dimensional propagation of shear waves is assumed, employing transfer function approaches based on SHAKE (e.g. in Sato et al. (1996) [32]; Yang and Yan (2009) [39]; Kaklamanos et al. (2013) [17]), time domain stick models (e.g. in Borja and Chao (1999) [5]) and Finite Element (FE) column models (e.g. in Li et al. (1998) [24]; Lee et al. (2006) [23]; Amorosi et al. (2010) [1]). Among the existing approaches for site response analysis, the FE method is the most versatile, as it allows the implementation of advanced constitutive models which can simulate realistically soil behaviour under seismic loading, the rigorous modelling of soil's fluid phase through hydro-mechanical (HM) coupling and the computation of the response in all three directions. However, the adoption of advanced numerical features requires validation against field data. In this respect, the data from downhole arrays of seismometers are particularly useful not only for the better understanding of the site response, but also for the validation and improvement of applied numerical procedures. Usually, the recorded motion at some depth of the profile is employed as the input motion for the analysis and the computed surface motion is compared against the monitored data for the validation of site response modelling. Such numerical analyses have been conducted by numerous researchers, such as the one-directional (1-D) applications of Muravskii and Frydman (1998) [27], Lee et al. (2006) [23] and Amorosi et al. (2010) [1] and the 3-D applications of Li et al. (1998) [24] and Borja et al. (1999) [5].

Typically, in 1-D site response analysis, a ground profile is subjected to the horizontal component of the seismic input motion, which is associated with the vertical propagation of shear waves. However, evidence of strong vertical ground motions and compressional damage of engineering structures have been increasingly observed in recent earthquakes (Papazoglou and Elnashai, 1996 [28]; Yang and Sato, 2000 [38]; Bradley, 2011 [7]). There is therefore a need for a systematic investigation of the site response subjected to both the horizontal and vertical components of the ground motion. The work of Li et al. (1998) [24], Borja et al. (1999) [5], Anantanavanich et al. (2012) [3], Motamed et al. (2015) [26], Amorosi et al. (2016) [2] and Tsaparli et al. (2016) [36] are representative examples of studies examining the soil response under multi-directional excitations.

One of the most challenging aspects of 3-D site response analysis is the accurate prediction of the vertical site response, mainly due to the sensitivity of the constrained modulus to several factors, such as the pore fluid compressibility, the water table location and the degree of unsaturation. Furthermore, a rigorous 3-D analysis requires a constitutive model with the ability to account for the coupling effects between shear and compressional response. Full 3-D FE analysis has been employed for multi-directional site response analysis, but in most cases only the horizontal component is rigorously investigated. For example, the 3-D site response analysis of Li et al. (1998) [24] predicted accurately only the horizontal component of the surface motion, while the reasons for the mismatch in the vertical direction have not been investigated in great detail. The site response at Lotung was satisfactorily predicted by Borja et al. (1999) [5] in all the three directions, but without considering HM coupling, which can further improve the predictions.

In this paper, the multi-directional seismic response at a downhole array site in Japan is simulated employing the 3-D dynamic nonlinear HM formulation of the Imperial College Finite Element Program (ICFEP, Potts and Zdravković (1999) [30]) aiming to accurately compute all three components of the ground motion. The paper discusses the challenges that 3-D modelling poses to the calibration of a cyclic nonlinear model, giving particular emphasis to the independent simulation of shear and volumetric deformation mechanisms. It should be noted that the detailed FE formulation of ICFEP can be found in Potts and Zdravković (1999) [30] for static conditions and in Kontoe (2006) [19] and Han et al. (2015a) [12] for dynamic conditions, which will not be discussed in the paper for brevity.

2 KiK-net downhole array observations

The KiK-net system is a well-established downhole array monitoring system in Japan, which includes 659 stations equipped with 3-D seismometers both at the ground surface and the base layer in a vertical array of a borehole. The site response of the HINO site subjected to the 2000 Western Tottori earthquake is chosen for the investigation in this paper, due to the strong intensity of the recorded ground motion at this site. The Western Tottori earthquake occurred at 13:30 JST (04:30 GMT) on 6th October, 2000 and its epicentre was located in western Tottori, south-west of Japan. According to the Japan

Meteorological Agency seismic intensity scale (JMA scale), the magnitude of the earthquake was M_w 7.3. The HINO site was the closest to the epicentre (6 km) among all the monitoring stations and consequently experienced high-intensity shaking, with the resultant peak ground acceleration (PGA) being 11.42m/s^2. Furthermore, another two after-shock weak motions at the HINO site are also selected for the investigation, whose peak accelerations are below 1 m/s^2 in all three directions.

The basic information for the three recorded earthquake events is listed in Table 1. At the HINO site, two 3-D seismometers are installed at the ground surface and the base layer (100 m below the ground level) of the downhole array. Earthquake motions were monitored during the three seismic events in three directions, denoted as east-west (EW), north-south (NS) and up-down (UD). The 3-D acceleration time histories recorded at the base layer during the three earthquakes are employed as the input motions for the subsequent 3-D numerical site response analyses, with their corresponding acceleration response spectra being shown in Figure 1.

The soil profile at the HINO site, consisting of gravel and silt overlaying weathered granite, is shown in Figure 2a, in terms of shear and compressional wave velocity variations. These data were based on P-S wave velocity logging tests obtained from the NIED (National Research Institute for Earth Science and Disaster Prevention) database. The water table is assumed to be at 10.4 m below the ground surface due to the significant increase of the compressional wave velocity at this depth (Beresnev et al. 2002 [4]). The material porosities are back-calculated based on the constrained modulus equation for saturated soils proposed by Zienkiewicz et al. (1980) [40], as shown in Equation (1):

$$M = \frac{E \cdot (1-\nu)}{(1+\nu) \cdot (1-2\nu)} + \frac{K_f}{n} = \frac{2G \cdot (1-\nu)}{1-2\nu} + \frac{K_f}{n} \tag{1}$$

where M and E are respectively the soil constrained and Young's moduli, ν is the Poisson's ratio, K_f is the bulk modulus for the pore water and n is the porosity. In particular, the constrained and shear moduli can be calculated based on the compressional and shear wave velocities, respectively. By assuming the Poisson's ratio to be 0.2 for the gravelly soil and weathered granite (Bowles, 1997 [6]), the porosities of the soil layers under the water table can be calculated. The porosity for the soil layer above the water table is assumed to be the same as the one in the layer beneath. The shear wave velocity profile at the HINO site was further investigated by Higashi and Abe (2002) [14] who conducted a seismic refraction test. In particular, based on the in-situ observations, the bedrock is

confirmed to be at 84m below the ground surface and a more precise shear wave velocity profile is obtained for the soil deposit in the top 10 m (see Figure 2b). This latter profile is employed in the subsequent FE analyses. However, the compressional wave velocities were not well investigated in Higashi and Abe (2002) [14]. Therefore, these are calculated based on Equation (1), where it should be noted that the pore fluid bulk modulus refers only to the medium constrained modulus below the water table. The mass density of the soil layers at the HINO site was based on Izutani (2004) [16] as shown in Figure 2b. The permeability of the weathered granite was assumed to be 1.0E-7 m/s, as suggested by Domenico and Schwartz (1990) [10] for a similar material, while the gravelly soils were assumed to be dry. Furthermore, an angle of shearing resistance of 35° was adopted for both the gravelly soils and the weathered rock as suggested by Bowles (1997) [6].

Table 1: Basic information of the three recorded earthquakes

	Date	**Time**	**Magnitude**	**Epicentre position**	**Site code**	**Site name**	**Site position**	**PGA (m/s^2)**	**Epicentral distance**
2000 Western Tottori earthquake	06/10 /2000	13:30 JST	7.3 M_w	35.28°N, 133.35°E	TTRH 02	HINO	35.23°N, 133.39°E	11.42	6.0 km
2001 Weak motion 1	11/02 /2001	09:17 JST	4.3 M_w	35.42°N, 133.29°E				0.43	23.0 km
2002 Weak motion 2	24/01 /2002	16:08 JST	4.5 M_w	35.36°N, 133.32°E				0.79	16.0 km

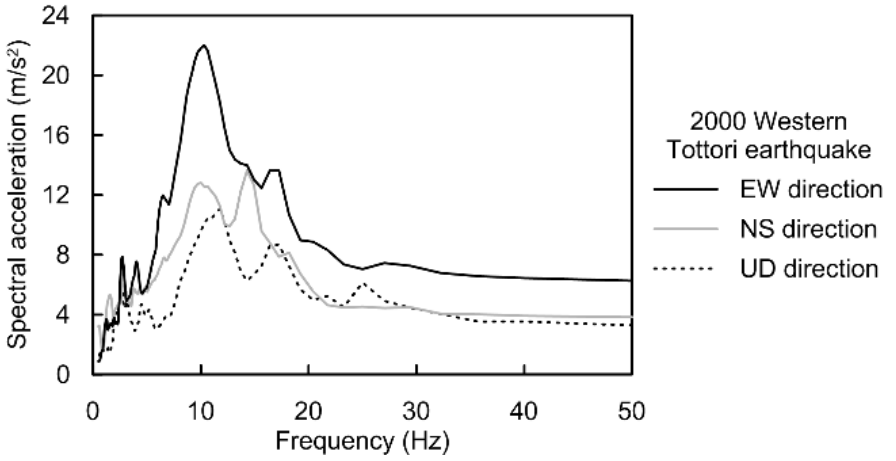

(a): 2000 Western Tottori earthquake

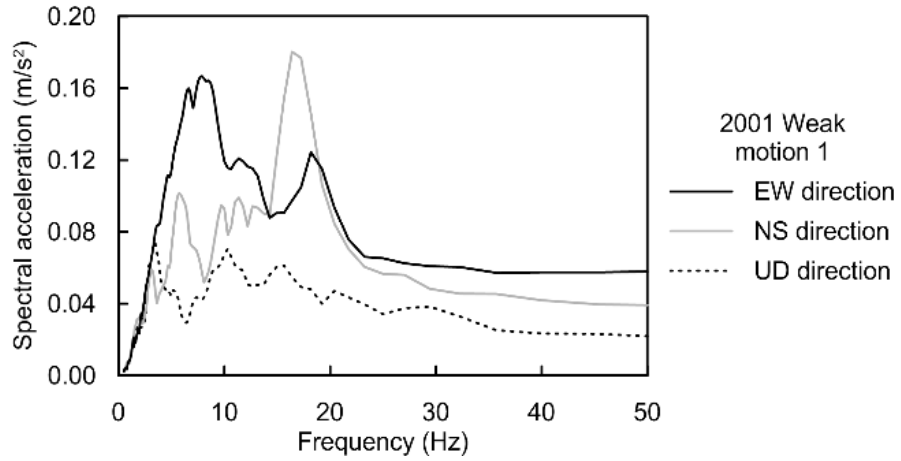

(b): 2001 weak motion 1

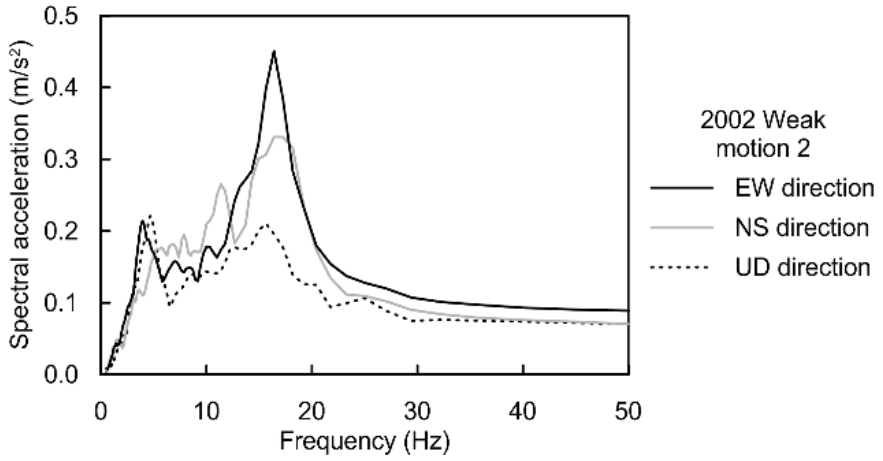

(c): 2002 weak motion 2

Figure 1: Acceleration response spectra of the observed response at the base layer of HINO site in three earthquake events (5% damping)

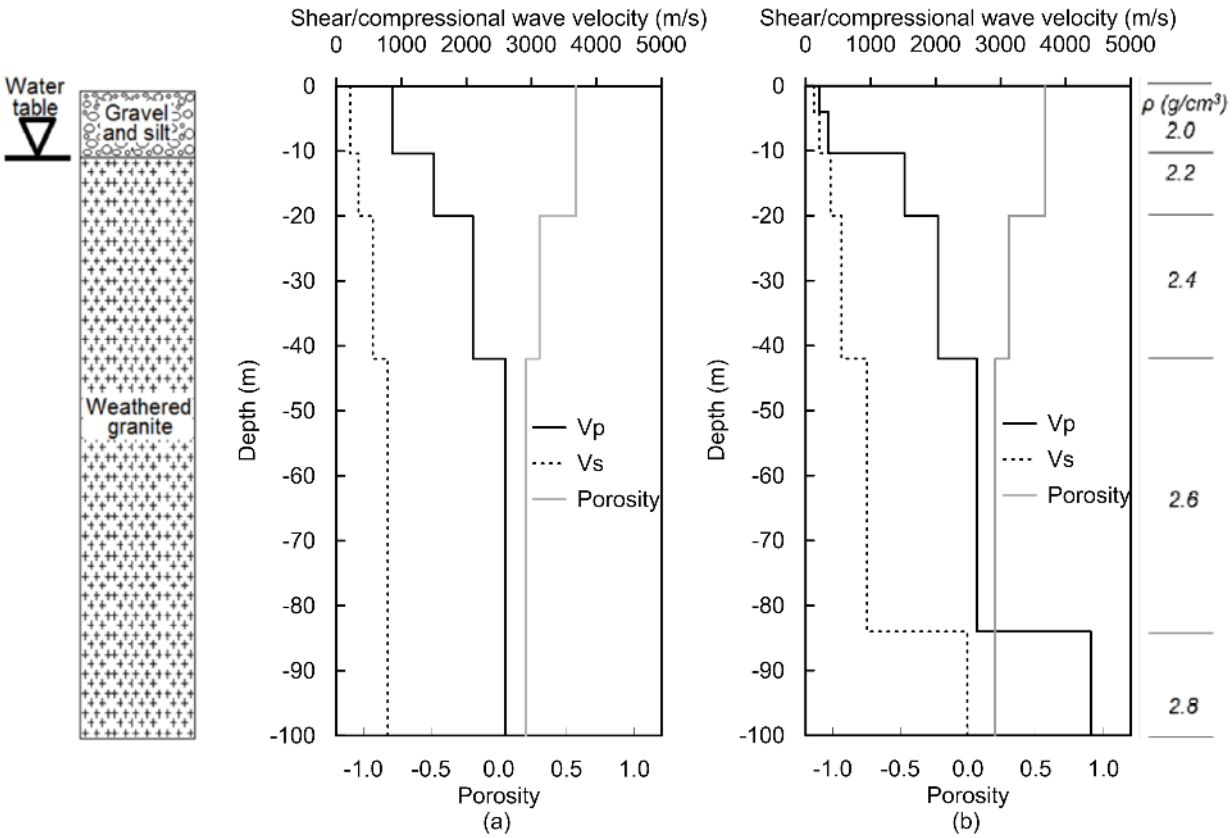

Figure 2: (a): Soil profile from NIED database (b): Soil profile adopted in FE analyses

3 Constitutive models employed for the site response analyses

Constitutive models for the simulation of the soil dynamic behaviour can be broadly categorised in three types; equivalent-linear models, cyclic nonlinear models and advanced elasto-plastic constitutive models. Equivalent linear models are widely employed in site response analysis, but their applicability is restricted in the small to medium strain range. On the other hand, advanced elasto-plastic models can simulate complex features of soil behaviour in terms of material nonlinearity, hardening/softening, excess pore water pressure accumulation, etc., but they require data from advanced laboratory tests for their calibration. A variety of cyclic nonlinear models have been proposed in the literature to simulate the nonlinear and hysteretic nature of soil behaviour, which are usually characterised by a backbone curve and several rules controlling loading and unloading, such as in Kondner and Zelasko (1963) [18], Matasovic & Vucetic (1993) [25] and Puzrin and Shiran (2000) [31]. A known feature of this class of models is the underestimation of the damping in the small-strain range and its overestimation in the large strain range. Studies have been conducted to overcome this limitation by

mathematically modifying the model formulations. Such effective work can be found in Puzrin and Shiran (2000) [31], Phillips and Hashash (2009) [29], Taborda and Zdravković (2012) [34], etc. In this study an advanced cyclic nonlinear model, the Imperial College Generalised Small Strain Stiffness model (ICG3S) of Taborda and Zdravković (2012) [34] and Taborda et al. (2016) [35] is combined with a Mohr-Coulomb failure criterion to simulate the soil response.

3.1 Imperial College Generalised Small Strain Stiffness model

The ICG3S model is based on the hyperbolic model by Kondner and Zelasko (1963) [18] and the modified hyperbolic model by Matasovic & Vucetic (1993) [25], but it involves additional rules to account for important aspects of soil behaviour, such as the independent simulation of shear and volumetric deformation mechanisms, spatial variation of soil stiffness and simulation of material damping at very small strain levels. The backbone curve for the ICG3S model is expressed by the integration of Equation (2), where G_{tan} and G_{max} are the tangent and maximum shear moduli, respectively, and *a*, *b* and *c* are model parameters. It should be noted that in order to account for soil nonlinear behaviour under general loading conditions, the 3-D strain invariant E_d is defined in Equation (3) (Potts and Zdravković, 1999 [30]). In the contrast, its modified counterpart E_d^* (expressed in Equation (4)), which assumes both positive and negative strain values (Taborda, 2011 [33]), is employed to describe the backbone curve in Equation (2).

$$\frac{G_{tan}}{G_{max}} = c + \frac{(1-c)}{1+\left(\frac{|E_d^*|}{a}\right)^b} \tag{2}$$

$$E_d = \frac{2}{\sqrt{6}}\sqrt{(\varepsilon_1-\varepsilon_2)^2+(\varepsilon_2-\varepsilon_3)^2+(\varepsilon_3-\varepsilon_1)^2} = \sqrt{\frac{4}{6}\left((\varepsilon_x-\varepsilon_y)^2+(\varepsilon_y-\varepsilon_z)^2+(\varepsilon_x-\varepsilon_z)^2\right)+\gamma_{xy}^2+\gamma_{yz}^2+\gamma_{xz}^2} \tag{3}$$

where ε_1, ε_2 and ε_3 are the principal strains, ε_x, ε_y and ε_z are normal strains in three orthogonal directions, γ_{xy}, γ_{yz} and γ_{xz} are the corresponding shear strains, *a*, *b* and *c* are model parameters. The parameters *a* and *b* control the shift and curvature of the backbone curve respectively, and the employment of smaller than 1 values for the parameter *c* limits the overestimation of damping at large strain levels.

$$E^{*}_{d,i+1} = E^{*}_{d,i} + N_{dir} \cdot \Delta E_d \tag{4}$$

where $E^{*}_{d,i+1}$ and $E^{*}_{d,i}$ are the modified 3-D strain invariants at steps i+1 and i respectively, ΔE_d is the incremental deviatoric strain and N_{dir} is a parameter which alternates between +1 and -1 to account for the reloading and unloading conditions respectively.

Most cyclic nonlinear models simulate hysteretic behaviour considering only the shear stiffness degradation, while bulk and constrained moduli are dependent on the shear modulus, assuming a constant Poisson's ratio, in terms of modulus degradation, material damping and reversal behaviour. However, the ICG3S model can independently reproduce the shear and volumetric deformation mechanisms. Therefore, a second backbone curve is specified for the volumetric response, expressed by the integration of Equation (5), where ε^{*}_{vol} is the volumetric strain, K_{tan} and K_{max} are the tangent and maximum bulk moduli, respectively, and *r*, *s* and *t* are another three model parameters, corresponding to parameters *a*, *b* and *c* for the backbone curve of the shear response. Furthermore, the reversal behaviour for shear and volumetric response are also independently simulated by numerically implementing different reversal control procedures. It should be noted that the material Poisson's ratio simulated by the ICG3S formulation is not constant and depends on the respective nonlinear states of the shear and bulk moduli. Therefore, the simulated Poisson's ratio values should be carefully checked during the numerical analyses in order to avoid unrealistic simulations.

$$\frac{K_{tan}}{K_{max}} = t + \frac{(1-t)}{1+\left(\frac{\left|\varepsilon^{*}_{vol}\right|}{r}\right)^{r}} \tag{5}$$

After introducing the basic Masing rules, the expressions for the ICG3S model are shown in Equation (6), where two scaling factors, n_1 and n_2, are employed for the shear and volumetric stress-strain hysteretic loops respectively. These two scaling factors are independently controlled by the model parameters d_1-d_4 and d_5-d_8. As mentioned before, the soil material damping at very small strain levels is generally underestimated by most existing cyclic nonlinear models when using a constant scaling factor of 2, as suggested by the original Masing rules. This can lead to a non-conservative assessment for dynamic analysis of geotechnical structures and limit the applicability of cyclic nonlinear models (Taborda and Zdravković, 2012 [34]). However, the employment of varying scaling

factors within the ICG3S model enables the more accurate simulation of the material damping in the very small strain range.

$$\begin{cases} \dfrac{G_{tan}}{G_{max}} = c + \dfrac{(1-c)}{1+\left(\dfrac{\left|E_d^* - E_{d,r}^*\right|}{n_1 a}\right)^b} \\ \dfrac{K_{tan}}{K_{max}} = t + \dfrac{(1-t)}{1+\left(\dfrac{\left|\varepsilon_{vol}^* - \varepsilon_{vol,r}^*\right|}{n_2 r}\right)^s} \end{cases} \tag{6}$$

where

$$\begin{cases} n_1 = (d_1+2)^{\left|E_d^* - E_{d,r}^*\right|^{d_2}} \left(\dfrac{(d_3+1)\left|E_d^* - E_{d,r}^*\right|}{1+(d_3+1)\left|E_d^* - E_{d,r}^*\right|}\right)^{d_4} \\ n_2 = (d_5+2)^{\left|\varepsilon_{v\,o}^* - \varepsilon_{v\,o,r}^*\right|^{d_6}} \left(\dfrac{(d_7+1)\left|\varepsilon_{v\,o}^* - \varepsilon_{v\,o,r}^*\right|}{1+(d_7+1)\left|\varepsilon_{v\,o}^* - \varepsilon_{v\,o,r}^*\right|}\right)^{d_8} \end{cases}$$

and $E_{d,r}^*$ and $\varepsilon_{vol,r}^*$ are the deviatoric and volumetric strain invariants at the reversal point.

Concerning the calibration for cyclic nonlinear models, usually the reproduced shear modulus degradation and damping curves are compared against corresponding laboratory data or empirical curves. This is sufficient for geotechnical structures subjected only to horizontal earthquake motions. However, for soil profiles subjected to 3-D earthquake motions, the vertical response is dependent on the soil constrained modulus. Therefore, it is also necessary to calibrate the cyclic nonlinear models based on constrained modulus degradation (M/M_{max}) and corresponding damping ratio curves. In order to obtain these curves, the vertical stress-strain loops are predicted based on the model formulation. In particular, the incremental vertical stress is calculated based on the incremental vertical strain and tangential constrained modulus. For cyclic nonlinear models that employ only the shear modulus, the tangential constrained modulus can be directly calculated based on the transient tangential shear modulus and Poisson's ratio at each shear strain level. In this case, the modulus degradation and damping curves for shear and compressional response are dependent on the same set of model parameters, and therefore the overall calibration of these models should consider an optimum degradation response in both modes of deformation. However, for cyclic nonlinear models that employ both shear and bulk modulus variations, the tangential constrained modulus can be calculated based on the shear and bulk moduli at each shear and volumetric strain levels respectively. In this case, modulus degradation and damping curves for shear and compressional response are

independently controlled by two sets of model parameters, which can be separately calibrated against the corresponding laboratory, field or empirical data. Taking the ICG3S model for example, the calibration for modulus degradation and damping curves of shear and compressional response are respectively controlled by parameters *a*, *b*, *c*, d_1 to d_4 and *r*, *s*, *t*, d_5 to d_8. The relationship between the vertical strain and shear strain, and the relationship between the vertical strain and volumetric strain are presented in Equation (7), where ε_h and ε_v represent the horizontal and vertical strains respectively. These two relations are derived based on the expression for the deviatoric strain in Equation (3) assuming triaxial test conditions of $\varepsilon_x = \varepsilon_y = \varepsilon_h$, $\varepsilon_z = \varepsilon_v$ and $\gamma_{xy} = \gamma_{xz} = \gamma_{yz} = 0$. Further assumption in Equation (7) is that $\varepsilon_h = 0$, due to the restricted lateral deformation when determining soil constrained modulus.

$$\begin{cases} E_d = \dfrac{2}{\sqrt{3}}\left(\varepsilon_v - \varepsilon_h\right) = \dfrac{2}{\sqrt{3}}\gamma \overset{\varepsilon_h=0}{=} \dfrac{2}{\sqrt{3}}\varepsilon_v \\ \\ \varepsilon_{vol} = \varepsilon_v + 2\varepsilon_h \overset{\varepsilon_h=0}{=} \varepsilon_v \end{cases} \tag{7}$$

3.2 Elasto-plastic yield surface

The previously described cyclic nonlinear model can only simulate the pre-yield elastic soil behaviour. In this paper, the ICG3S model is coupled with Mohr-Coulomb model for plasticity. Plastic deformations can be generated only when the stress state reaches the Mohr-Coulomb yield surface. The expression for the Mohr-Coulomb yield function, as implemented in ICFEP, is shown in Equation (8).

$$F = J - \left(\frac{c'}{\tan\phi'} + p'\right) g(\theta) = 0 \tag{8}$$

where

$$J = \frac{1}{\sqrt{6}}\sqrt{\left(\sigma_1' - \sigma_2'\right)^2 + \left(\sigma_2' - \sigma_3'\right)^2 + \left(\sigma_3' - \sigma_1'\right)^2} = \sqrt{\frac{1}{6}\left(\left(\sigma_x' - \sigma_y'\right)^2 + \left(\sigma_y' - \sigma_z'\right)^2 + \left(\sigma_x' - \sigma_z'\right)^2\right) + \tau_{xy}^2 + \tau_{yz}^2 + \tau_{xz}^2}$$

$$p' = \frac{1}{3}\left(\sigma_1' + \sigma_2' + \sigma_3'\right)$$

$$\theta = \frac{1}{\sqrt{3}}\left(2\frac{\sigma_2' - \sigma_3'}{\sigma_1' - \sigma_3'} - 1\right)$$

$$g(\theta) = \frac{\sin\phi'}{\cos\theta + \frac{\sin\theta\sin\phi'}{\sqrt{3}}}$$

where J is the generalised deviatoric stress in the form of the second invariant of the stress tensor, σ_1', σ_2' and σ_3' are the principal effective stresses, σ_x', σ_y' and σ_z' are the normal effective stresses in three orthogonal directions, τ_{xy}, τ_{yz} and τ_{xz} are the corresponding shear stresses, p' is the mean effective stress, c' is the soil material cohesion, ϕ' is the angle of shearing resistance, θ is the Lode's angle and $g(\theta)$ defines the shape of the yield surface on the deviatoric plane. It is noted that there is no direct evidence from laboratory tests showing the dilatant behaviour of the investigated materials and therefore a zero angle of dilatancy was assumed in the analyses.

4 Multi-directional site response analysis subjected to two weak earthquake motions

The 3-D site response of the HINO site is first investigated for the two weak earthquake motions to validate the numerical procedures in the low strain range. In order to compensate for the inability of cyclic nonlinear models to generate damping in the small strain range, Rayleigh damping is usually employed in nonlinear analysis. However, Rayleigh damping is only an approximate way to reproduce material damping, as it is not related to the induced strain level, is strongly frequency-dependent and its implementation in nonlinear analysis is problematic as the target damping ratio calculation is based on the elastic stiffness (Kontoe et al., 2011 [21]). However, for the present site response analyses, no Rayleigh damping was employed and therefore the simulation of the response for the two weak motions will clearly test the ability of the ICG3S model to reproduce damping in the small strain range.

4.1 Numerical model

The FE mesh of the HINO site, consisting of 400 20-noded isoparametric hexahedral

elements, and the adopted boundary conditions are shown in Figure 3. The dimensions of the FE mesh are 2m, 2m and 100m in the X, Z and Y directions, respectively, which represent the corresponding EW, NS and UD directions of the HINO site. 3-D tied degrees-of-freedom (DOF) boundary conditions are employed on the lateral boundaries in both the EW and NS directions. In particular, the DOFs of displacement and pore water pressure at nodes at the same elevation but in opposite lateral boundaries are tied to be identical. The value of pore water pressure at the water table surface boundary is prescribed as zero and is not allowed to change throughout the analysis (i.e. Δp=0). The bottom boundary is considered to be impermeable (i.e. no flow across the boundary). Regarding the initial stresses applied in the numerical analyses, zero and hydrostatic pore water pressures are assumed for the materials above and below the water table respectively. Furthermore, static self-weight are prescribed through the whole deposit, where the coefficient of earth pressure at rest (K_0) is applied to be 0.5. The Generalised-α time integration method (CH method), proposed by Chung & Hulbert (1993) [8] and extended for the HM coupled formulation in ICFEP by Kontoe 2006 and Kontoe et al. (2008) [20], is utilised for the FE analyses. The employed time integration parameters, i.e. the Newmark method parameters δ and α, CH method parameters α_m and α_f and consolidation parameter β, are listed in Table 2, which satisfy the stability conditions of the CH method under HM coupled formulation, proposed by Han (2014) [11] and Han et al. (2015a) [12]. The 3-D acceleration time histories recorded at the base layer of the HINO downhole during two weak aftershocks of the Western Tottori earthquake, are uniformly prescribed at the bottom boundary of the mesh as the input motion. The soil properties employed in the numerical analyses are shown in Figure 2b. Soil below the water table is considered as HM coupled, while that above is treated as a drained material.

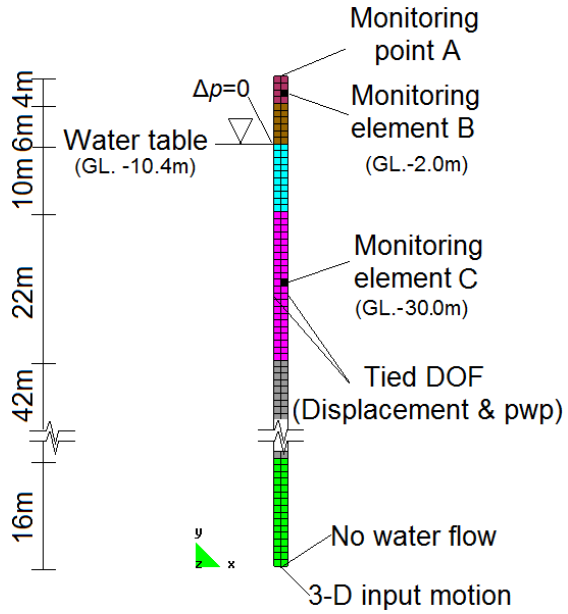

Figure 3: FE model for the HINO site

Table 2: The integration parameters for the CH method employed in site response analyses

Parameter	δ	α	α_m	α_f	β
CH method	0.93	0.51	-0.14	0.29	0.8

The parameters of the ICG3S model are calibrated by comparing the reproduced modulus degradation and damping curves against empirical curves and the results from in-situ tests in Figure 4. In particular, for the calibration associated with the shear response, the empirical shear modulus degradation and damping curves proposed by Imazu and Fukutake (1986) [15] are employed for the gravelly materials at the HINO site (shown as the solid and dashed grey lines in Figure 4a respectively). It should be noted that these empirical curves were also utilised by Izutani (2004) [16] to investigate the site response at the HINO site using a 1-D shake-type analytical solution, achieving a reasonable prediction.

However, due to the limited investigation on strain-dependent variation of the constrained modulus, there is a lack of data for the calibration of cyclic nonlinear models associated with the compressional/volumetric response. Only recently such work was attempted by LeBlanc et al. (2012) [22] using an in-situ testing apparatus (the large mobile shaker), and by Han et al. (2015b) [13] analysing seismic in-situ records. From LeBlanc et al. (2012) [22], constrained modulus degradation curves were proposed under

different total vertical confining pressures (σ_v). It was observed that in the vertical confining pressure range 28-50kPa, the soil constrained modulus exhibits clear degradation as the axial strain increases. It should be noted that the degradation curve under the condition of the maximum vertical stress (50kPa) was found to be in agreement with the degraded constrained moduli of the HINO site materials in the strain range of 0.0005%-0.01% as back-analysed from the monitored data for a strong earthquake event (Beresnev et al. 2002 [4]). Therefore, this curve (the solid grey line shown in Figure 4b is selected for the calibration of the cyclic nonlinear model associated with the compressional response. However, due to the limited investigation, there is no available data for the calibration of the material damping related to compressional soil response, which will depend on the calibration of the constrained modulus.

It was mentioned before that the ICG3S model can independently simulate the shear and compressional soil behaviour by specifying two sets of parameters (Equation (6)). In order to highlight the effects of this numerical feature on simulating multi-directional site response, in the subsequent numerical investigations, a simplified version of the ICG3S model is also utilised, which employs a variation for the shear modulus with cyclic shear strains and a constant Poisson's ratio. This essentially implies that an identical degradation is adopted for the constrained modulus and this version of the model is denoted herein as the ICG3S-1 model, while the full version is designated as ICG3S-2 model. The calibrated model parameters for the nonlinear FE analysis are listed in Table 3, where it should be noted that the second set of parameters is only employed for the independent modelling of the shear and compressional deformation mechanisms (i.e. only for the ICG3S-2 model). Calibrated curves of both ICG3S models are shown in Figure 4. This figure shows that identical shear modulus degradation and damping curves are predicted by the two models, as the same parameters which control the shear response are employed. On the other hand, the ICG3S-2 model allows the independent calibration for constrained modulus against the reference curve proposed by Leblanc et al. (2012) [22], achieving a better agreement than the ICG3S-1 model.

Furthermore, by employing varying scaling factors (i.e. n_1 and n_2 in Equation (6)), the ICG3S model enables a more adequate simulation of the material damping in the very small strain range (10^{-5} %-10^{-3} %). At extremely small strain levels (<10^{-5} %), the material damping simulated by the ICG3S model still starts from zero. This under-prediction cannot be mathematically avoided in cyclic nonlinear model formulations. However, such

low deformations are typical of extremely small oscillations, which are not within the range considered in geotechnical earthquake engineering problems. It should be noted that the material damping of the shear response at higher strain levels (>10^{-3} %) is over-estimated by the ICG3S model, compared with the empirical curves. However, this can be practically ignored for the analyses of the weak earthquake motions, as high strain levels are not mobilised.

It is noteworthy that cyclic nonlinear models usually overestimate the damping ratio at large strain levels (>10^{-1} %) (Puzrin and Shiran, 2000 [31]; Phillips and Hashash [29], 2009; Taborda, 2011 [33]). To alleviate this shortcoming, in the ICG3S model, values smaller than 1 for the parameters *c* or *t* are adopted to reach a more accurate damping prediction at large strain levels. In particular, as illustrated in Figure 4, the predicted damping ratio increases at small and intermediate strain levels and decreases at large strain levels. Therefore, the model essentially overestimates damping at intermediate strain levels, while underestimating it at large strain amplitudes. This issue can be overcome by a careful calibration procedure by achieving an optimum damping prediction in the concerned deformation range, as suggested in Taborda (2011) [33]. A quick estimate of the strain level of interest for a particular ground motion can be obtained by considering the ratio of the peak particle velocity of the input ground motion over the shear wave propagation velocity of the material under consideration. Alternatively, for a better estimate of the strain level, an equivalent linear site response analysis can be performed prior to the calibration of the nonlinear model. Furthermore, this procedure (i.e. adopting *c* or *t* values lower than 1) also avoids the unrealistic excessive reduction of the material moduli (i.e. G_{tan} or K_{tan} close to zero) in the large strain range. The soil damping reduction at high strain levels is also predicted when employing the empirical damping formulation proposed by Darendeli (2001) [9], particularly for lower plasticity index (I_P) values, and other cyclic nonlinear models such as the one presented by Puzrin and Shiran (2000) [31] for c<1.0. Indeed, there is currently a considerable lack of experimental data on damping ratio values for strain levels above 1%, which can support this pattern of soil damping variation at high strain levels.

Table 3: Parameters of the ICG3S model for the nonlinear analysis subjected to the weak motions

Parameters for the shear response						
a	b	c	d_1	d_2	d_3	d_4
5.00E-04	4.00E+00	5.00E-02	7.28E+01	2.28E-01	6.77E+02	7.58E-01
Parameters for the compressional response						
r	s	t	d_5	d_6	d_7	d_8
5.00E-04	8.00E+00	5.00E-02	7.28E+01	2.28E-01	6.77E+02	7.58E-01

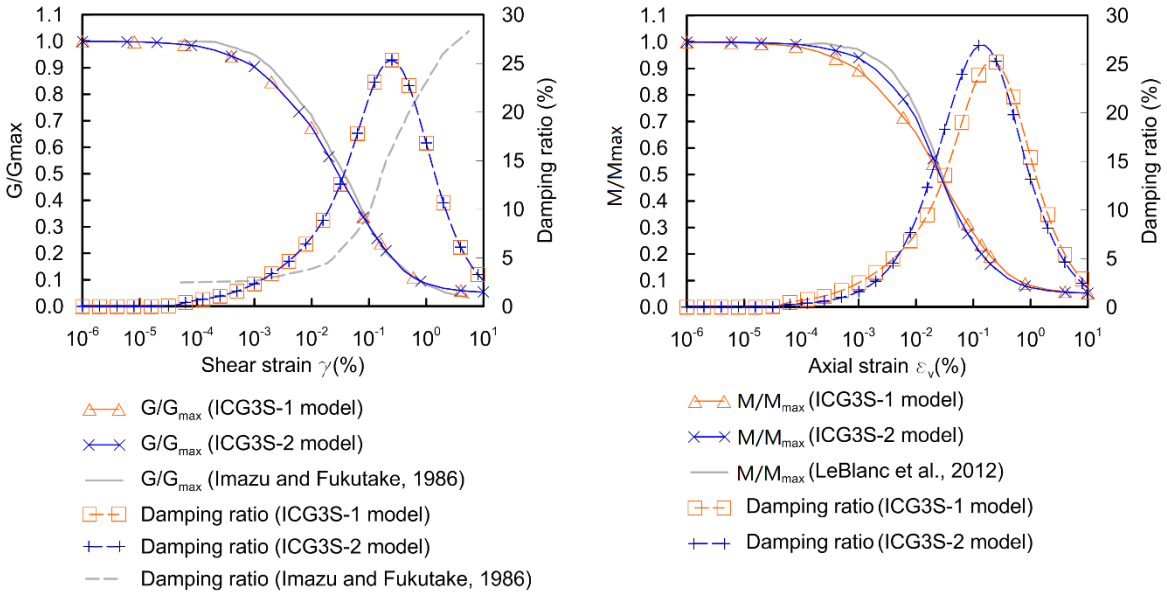

(a): Shear response (b): Compressional response

Figure 4: Calibration of the ICG3S model for the nonlinear analysis

4.2 Numerical results

The 3-D site response at the HINO downhole predicted by the FE analysis employing the ICG3S-2 model is compared against the monitored data of the two weak earthquake motions, in terms of the acceleration response amplification spectra between the top (point A) and the bottom boundary, in Figures 5 and 7, and in terms of acceleration time histories at monitoring point A in Figures 6 and 8. The spectral acceleration ratios are calculated by dividing the response spectra obtained at point A by the spectra at a corresponding point at the bottom boundary over the frequency range. It can be seen that overall the numerical predictions compare well with the monitored data, in terms of frequency content, amplification and acceleration time histories. In particular, based on the numerical results for weak motion 1 (Figure 5), the fundamental frequencies are

estimated to be 2.5Hz, 2.5Hz and 5.9Hz for the EW, NS and UD directions respectively, which are in very good agreement with the ones obtained from the monitored data. This agreement implies that the adopted small strain soil properties for the site response analyses are realistic. Concerning the site response for weak earthquake motion 2 (Figure 7), the fundamental frequencies are estimated as 2.5Hz, 2.5Hz and 6.0Hz for EW, NS and UD directions respectively, which match closely with the ones predicted for weak motion 1.

However, FE analyses slightly overestimate the amplification factors at the fundamental frequencies in the EW and UD directions of weak motion 1 and in the EW direction of weak motion 2. The overestimated acceleration response is due to a small underestimation of material damping at very small strain levels by the ICG3S model. In any case though, the underestimation of the response is minor and overall the ICG3S model offers an improved representation of damping in the small strain range considering that no additional viscous damping was employed.

Figures 5 and 7 further compare the predictions of the ICG3S-1 and -2 models in terms of acceleration response amplification spectra. Significant differences are observed in the vertical component (UD) of the predicted site response. In particular, the fundamental frequencies of the vertical site response are underestimated by the nonlinear analysis employing the ICG3S-1 model, particularly for weak motion 2. This can be attributed to the inadequate modelling of the constrained modulus degradation shown in Figure 4. The fundamental frequencies predicted by the ICG3S-2 model are larger and therefore agree better with the monitored data. This is a consequence of the adopted independent calibration of the constrained modulus, which is more accurate when compared against the reference curve (as shown in Figure 4).

It should be noted that the numerical analysis does not predict accurately the second amplification peak in the NS direction for weak motion 2, which is found to be at 6Hz. However, the numerical predictions for both weak motions and the observed data for weak motion 1 all show that the second amplification peak is approximately at 4.5Hz. Consequently, it is difficult to explain the origin of the second peak in the amplification response spectra of the recorded weak motion 2.

To conclude, the numerical results show that the multi-directional site response subjected to the two weak motions is reasonably well simulated by the FE analysis

employing the ICG3S-2 model, when compared with the monitored response. In particular, compared to its simplified version, the ICG3S-2 model is able to accurately predict both the horizontal and vertical site response by independently controlling the degradation of the shear and the constrained modulus. Furthermore, the agreement with the recorded response indicates that this model is adequate to simulate realistically the material damping at very small strain levels.

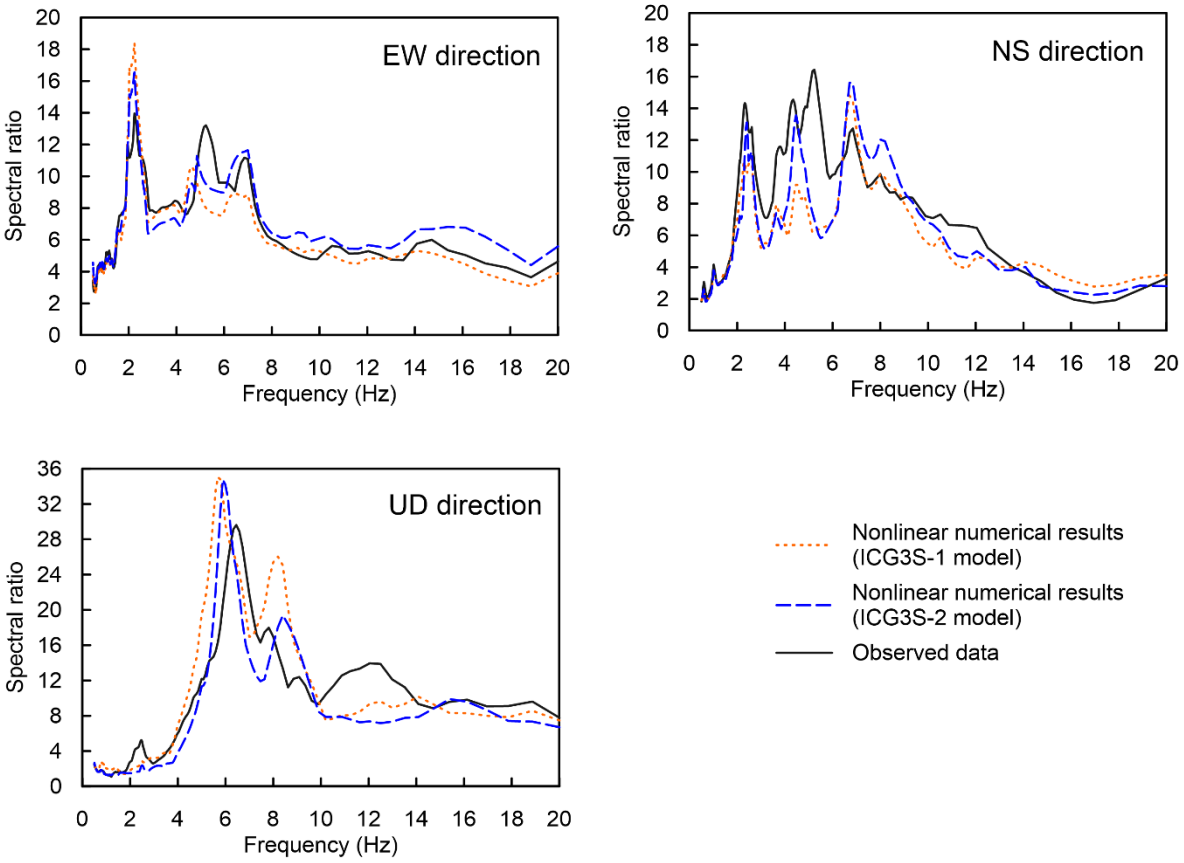

Figure 5: Nonlinear analysis results under weak earthquake motion 1 (response amplification spectra)

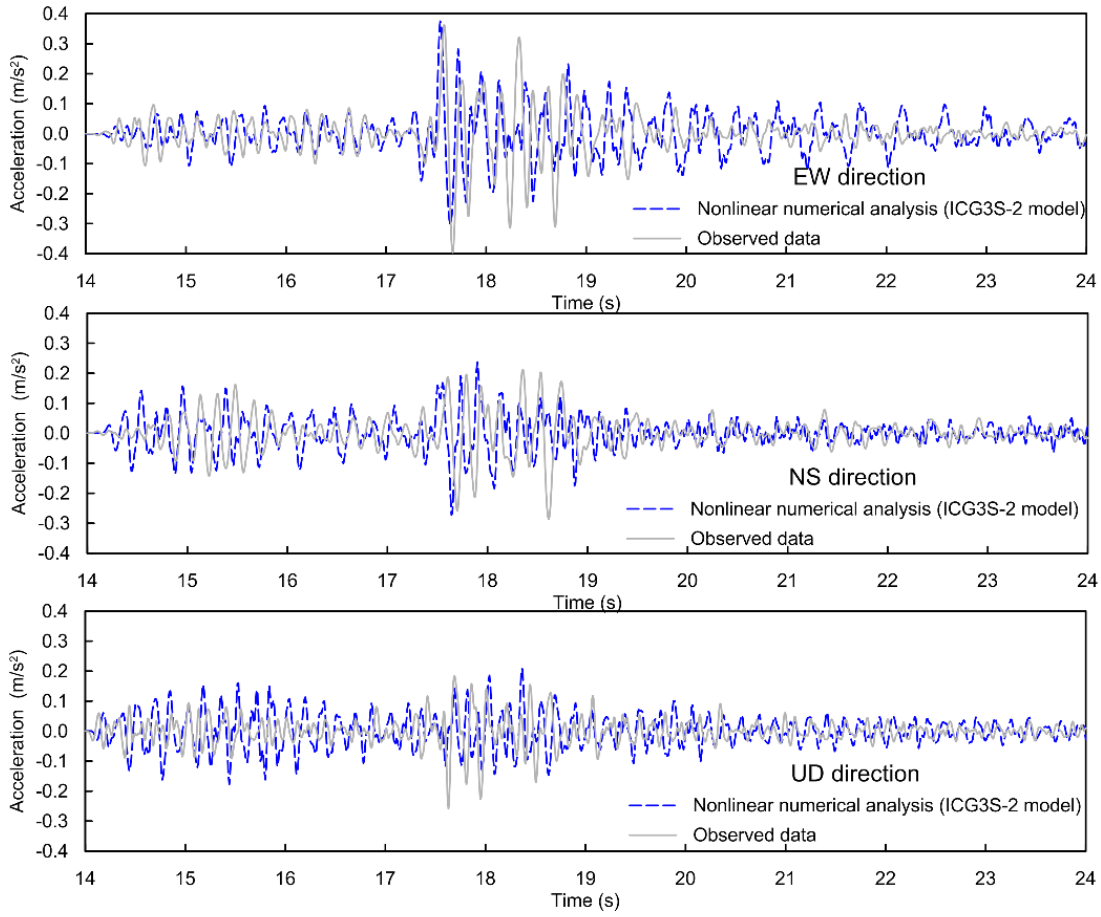

Figure 6: Nonlinear analysis results under weak earthquake motion 1 (acceleration time histories)

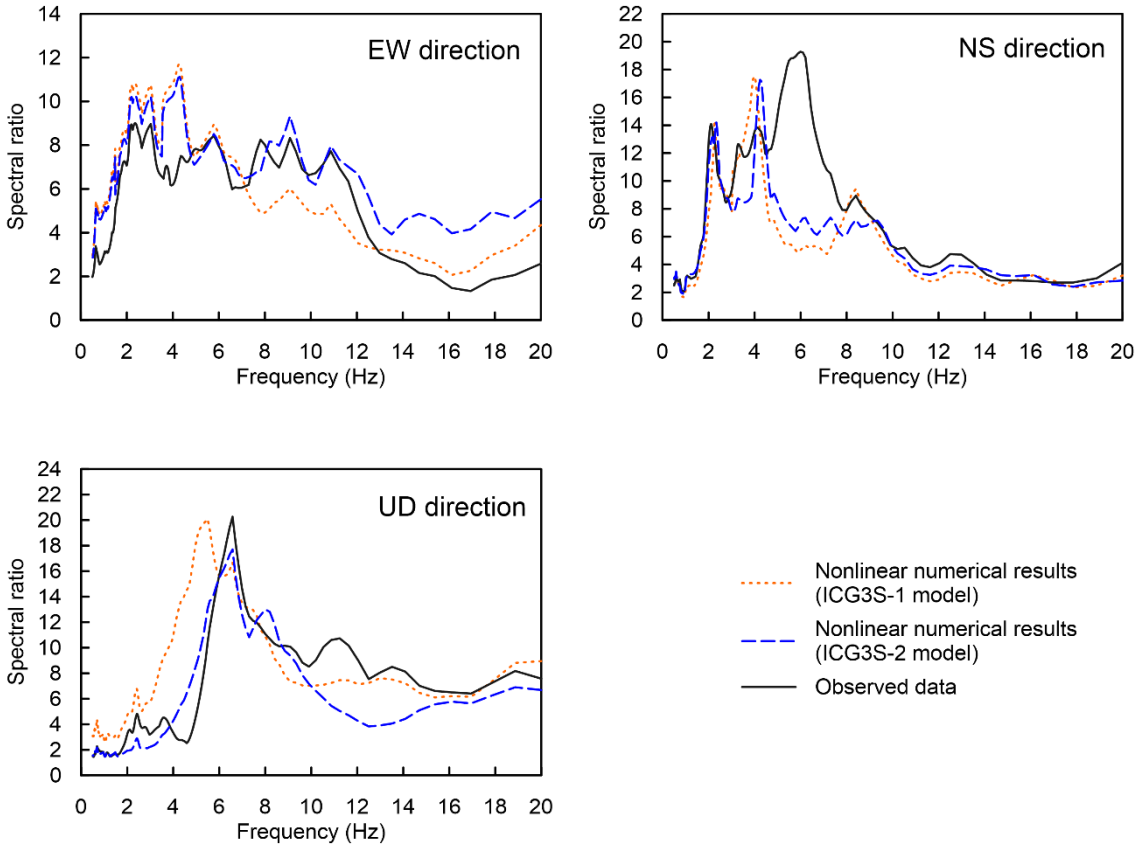

Figure 7: Nonlinear analysis results under weak earthquake motion 2 (response amplification spectra)

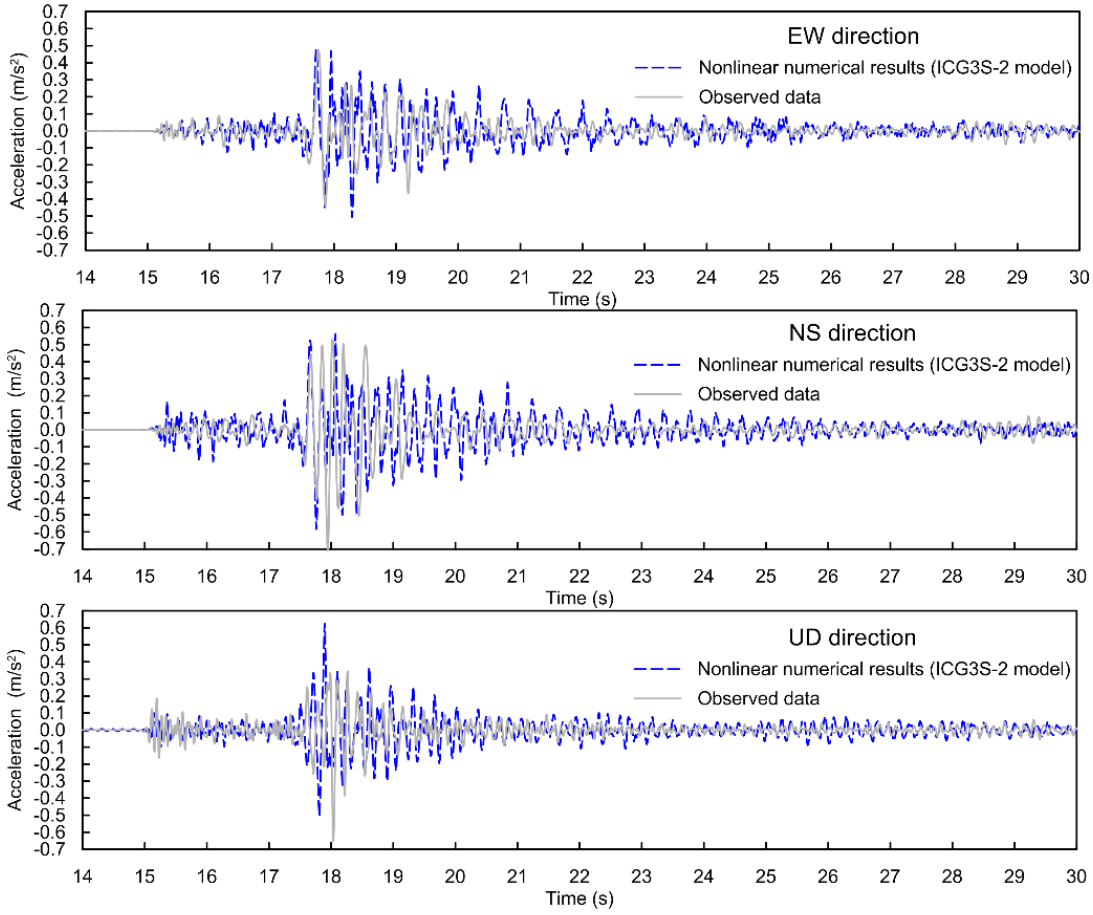

Figure 8: Nonlinear analysis results under weak earthquake motion 2 (acceleration time histories)

5 Multi-directional site response analysis subjected to the 2000 Western Tottori earthquake

5.1 Numerical model

In this part, the site response of the HINO site subjected to the main earthquake motion of the 2000 Western Tottori earthquake is simulated by 3-D nonlinear HM coupled FE analysis. The soil properties, FE mesh, boundary conditions and time integration method are the same as those employed in the previous section. The strong motion monitored at the base layer of the HINO downhole on 06/10/2000 is uniformly prescribed at the bottom boundary of the FE mesh as the input motion for the site response analysis.

Both ICG3S-1 and -2 models are employed to investigate the effects of the independent simulation of shear and compressional deformation mechanisms on predicting multi-directional site response. The ICG3S-1 model parameters are the same as those employed for the weak motion analyses, as listed in Table 3. However, the present calibration of the

ICG3S-2 model is different to the one employed for the two weak motions. The new model parameters are listed in Table 4 and the corresponding calibration curves are compared with the ones for the weak motions in Figure 9. The revised calibration for the larger intensity motion was deemed necessary because the ICG3S model, as most cyclic nonlinear models of this class, cannot represent the damping curve well for the entire strain range simultaneously. In particular in Figure 9, for the calibration curves of the weak motions, when γ is smaller than 10^{-3} %, the ICG3S-2 model provides hysteretic damping to account for the material energy dissipation at very small strain levels. However, at larger strain levels (greater than 10^{-3} %), the material damping related to the shear response is overestimated by the ICG3S-2 model compared with the empirical curves. For weak earthquake motions, this over-prediction of the damping can be practically ignored, since only low-magnitude soil deformation is triggered. For strong earthquake motions, larger soil deformation can be generated. Therefore, as shown in Figure 9, the present damping calibration curves associated with the shearing response are improved and match better with the empirical curve at high strain levels compared with the weak motion ones. In this way an optimum calibration is achieved in the concerned range of the strong earthquake motion. On the other hand, since vertical motions are usually of low intensity compared to the horizontal ones, the vertical soil deformation can be smaller. This requires the model to accurately simulate the damping associated with the compressional response at very small strain levels. These different requirements of the optimum damping calibrations associated with the shear and compressional response can only be satisfied when these two modes of deformation are independently controlled, i.e. by the ICG3S-2 model. Furthermore, Figure 9 shows again that, compared to the calibration of the ICG3S-1 model in Figure 4, both the reproduced shear and constrained modulus degradation curves can match well with the empirical curves due to the independent calibration for the two modes of deformation when using the ICG3S-2 model.

Table 4: Parameters of the ICG3S-2 model for the nonlinear analysis subjected to the strong motion

a	b	c	d_1	d_2	d_3	d_4
1.00E-04	8.00E-01	5.00E-02	0.00E+00	0.00E+00	0.00E+00	0.00E+00
r	s	t	d_5	d_6	d_7	d_8
5.00E-04	8.00E+00	5.00E-02	7.28E+01	2.28E-01	6.77E+02	7.58E-01

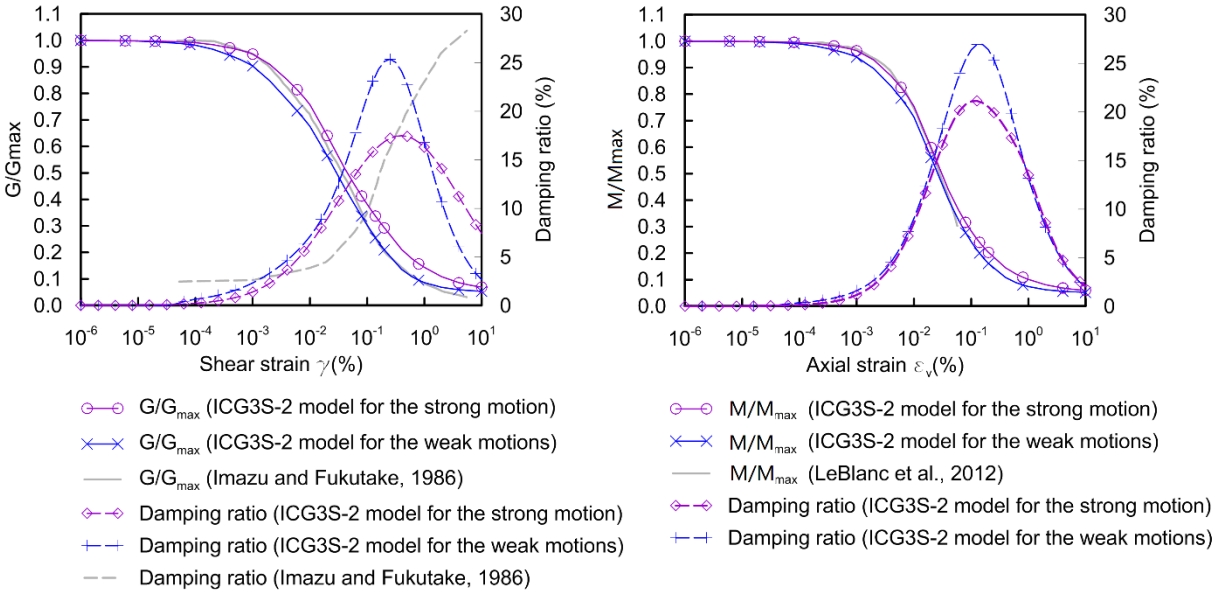

(a): Shear response (b): Compressional response

Figure 9: Calibration of the ICG3S model for the nonlinear analysis subjected to the strong motion

5.2 Numerical results

The numerically predicted 3-D site response of the HINO site employing the ICG3S-2 model is shown in Figures 10 and 11, in terms of the acceleration response amplification spectra between the top (point A) and bottom boundary and acceleration time histories at monitoring point A, respectively. Figure 10 further compares the predictions of ICG3S-1 and -2 models in terms of acceleration response amplification spectra. The horizontal site response in both the EW and NS directions is under-predicted by the ICG3S-1 model, where in particular the amplification factors in the frequency range between 1.7 Hz and 4.0 Hz are considerably smaller than the monitored data. It should be reminded that the same calibrated ICG3S-1 model could predict well the horizontal site response subjected to the two weak motions (as shown in Figures 5 and 7). This discrepancy of the strong

motion prediction is due to its inability of simultaneously achieving the optimum damping calibrations associated with the shear and compressional responses in their respective concerned strain ranges. Therefore, when employing the ICG3S-2 model, the amplification factors in the two horizontal directions in the frequency range between 1.7 Hz and 4.0 Hz are more accurately predicted, showing a better agreement with the recorded response. Furthermore, the prediction of the vertical site response is also improved by the ICG3S-2 model. The improvement on the prediction of the multi-directional site response is attributed to the adopted independent calibration of the constrained modulus. Overall, compared to the ICG3S-1 model, the ICG3S-2 model predicts reasonably well the 3-D site response of the HINO site subjected to the Western Tottori earthquake, in terms of both the acceleration response amplification spectra (Figure 10) and acceleration time histories (Figure 11). The comparison with the recorded response highlights the significance of the independent simulation of shear and compressional deformation mechanisms on improving the numerical predictions of multi-directional site response. It should be recognised though that two distinct calibrations were adopted (i.e. one for the weak motion and one for the strong motion), to achieve the optimum representation of stiffness and damping for the strain range of interest each time. This approach is essential for most cyclic nonlinear models to mitigate their inability to represent simultaneously well the stiffness and the damping for the entire strain range.

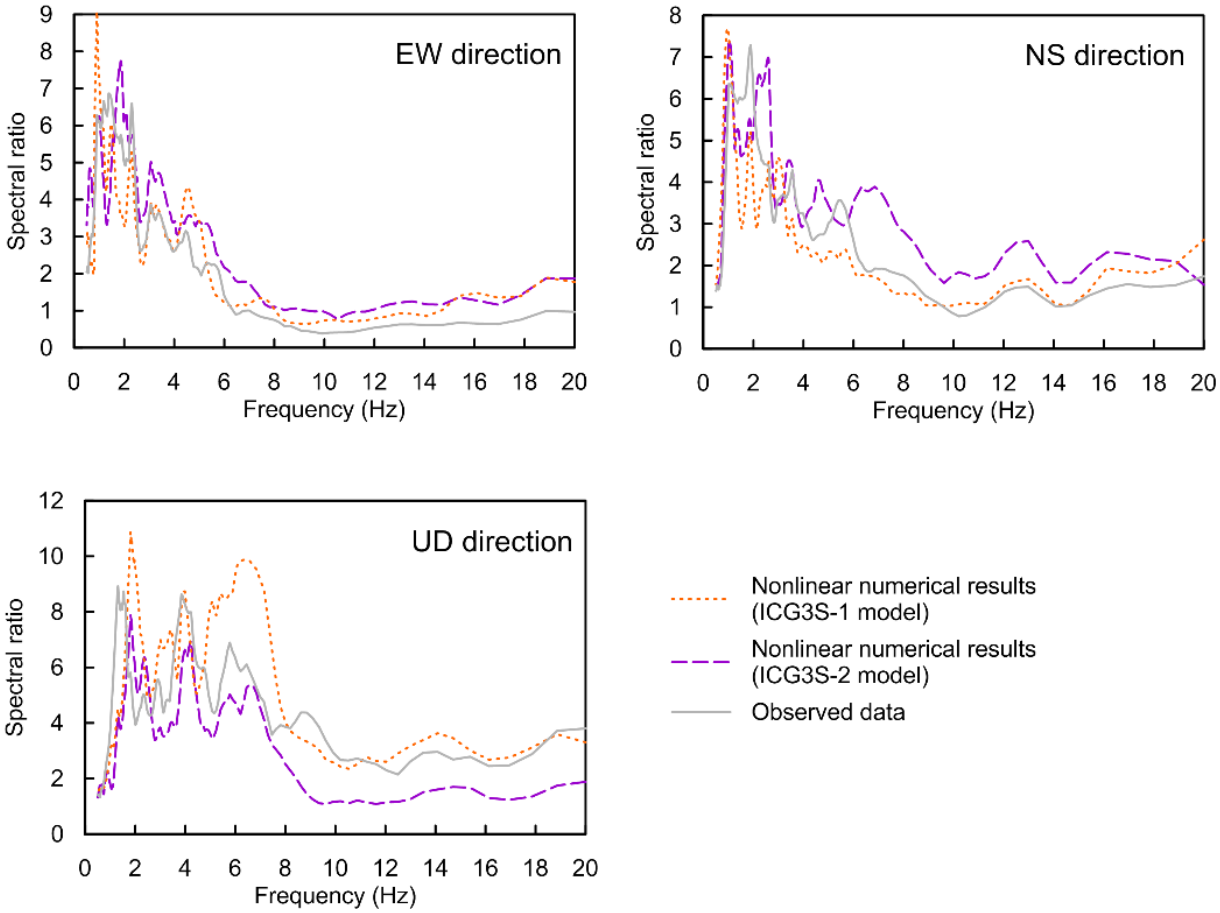

Figure 10: Nonlinear analysis results under Western Tottori earthquake (response amplification spectra)

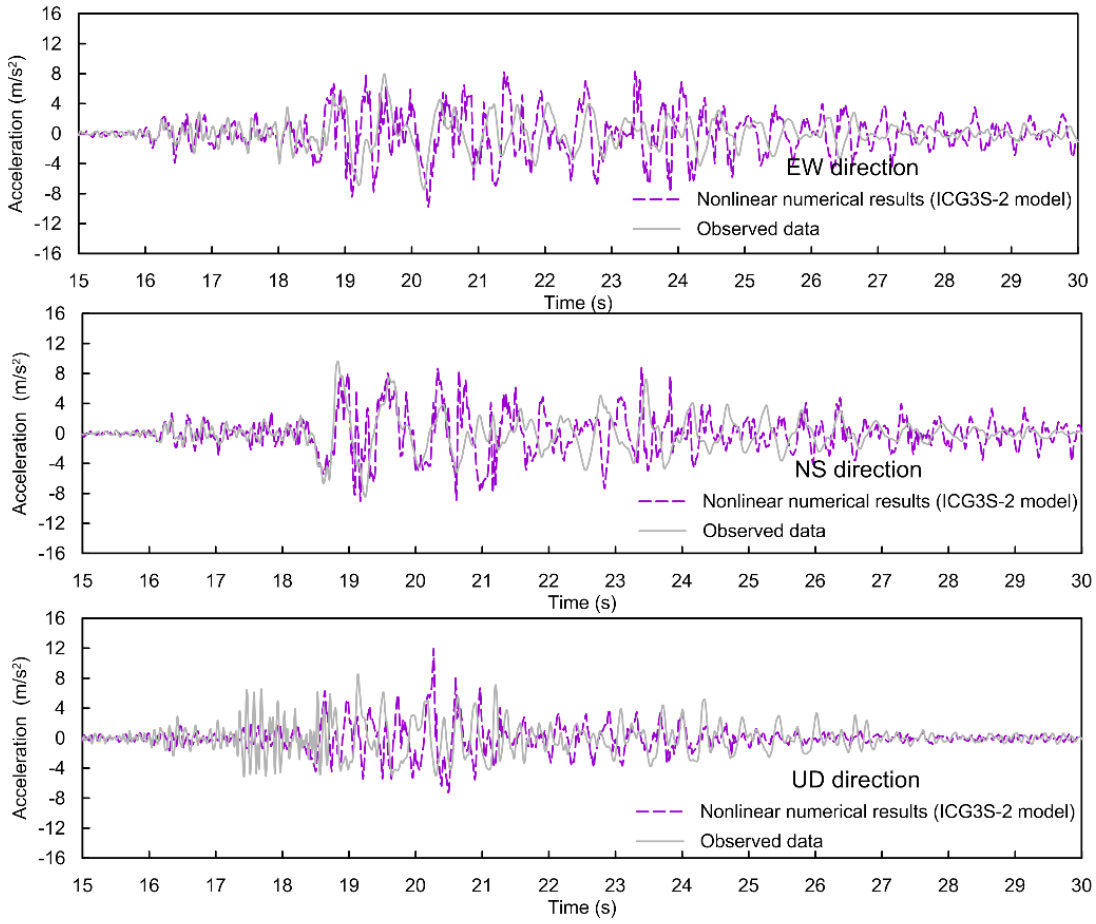

Figure 11: Nonlinear analysis results under Western Tottori earthquake (acceleration time histories)

By comparing the acceleration response amplification spectra of the strong and weak motions (comparison between Figures 10 and 5), the effect of soil nonlinearity can be depicted for all the three directions when subjected to the strong earthquake motion. In particular, the fundamental frequencies in the three directions are observed as 1Hz, 1Hz and 2Hz respectively, which are 40%, 40% and 33% of the ones for the weak motions. This implies significant degradation for both the shear and constrained moduli of the HINO site. Furthermore, the modulus degradation ratio time histories from the strong motion (G_{tan}/G_{max} and M_{tan}/M_{max}) are calculated for the elements at different depths and the time-average degradation ratios for each element are plotted with depth in Figure 12. It can be seen that the shear and constrained moduli degrade more significantly in the top 10 meters, while thereafter the degradation gradually reduces with depth. This is due to the low compressional wave velocities for the layers above the water table, which lead to larger vertical strains and therefore more significant constrained modulus degradation. As mentioned before, very few studies have investigated the strain-dependent variation of

the constrained modulus, and therefore there is a lack of data for the calibration of cyclic nonlinear models associated with the compressional/volumetric response. This is mainly due to the assumption that the compressional soil deformation is relatively small and the associated nonlinearity in the response is insignificant. However, based on the results shown in Figure 12, under strong earthquakes, the induced compressional nonlinearity cannot be neglected and can highly affect the multi-directional response. This indicates the necessity of experimentally investigating the compressional nonlinear soil behaviour to provide data for the model calibration of multi-directional nonlinear site response analysis.

The larger deformations in the soil layer above the water table are also reflected in the presented stress-strain response for two monitoring elements (element B and C in Figure 3) in Figure 13. Elements B and C are located at depths of GL. -2.0m and -30.0m, which are in the gravel and weathered granite materials, respectively. Larger strain levels are predicted at element B for all three directions, compared with that of element C.

Element C is located in the middle layer of the HINO site and the predicted deformations can approximately represent an average level for the whole layer. The maximum shear strain at element C is approximately 0.2% (Figure 13a). Plastic shear deformation is triggered during the dynamic analysis, indicated by the plastic strain time histories of element C shown in Figure 14. This shows that, when subjected to strong motions, the damping curves related to the shear deformation require an accurate calibration at medium to large strain levels (i.e. $>10^{-1}$ %). Furthermore, the maximum vertical strain at the element C is approximately 0.004% (Figure 13c) and no plastic vertical deformation is predicted (Figure 14). Hence, the damping curves associated with the compressional response need to achieve an accurate calibration at very small strain levels.

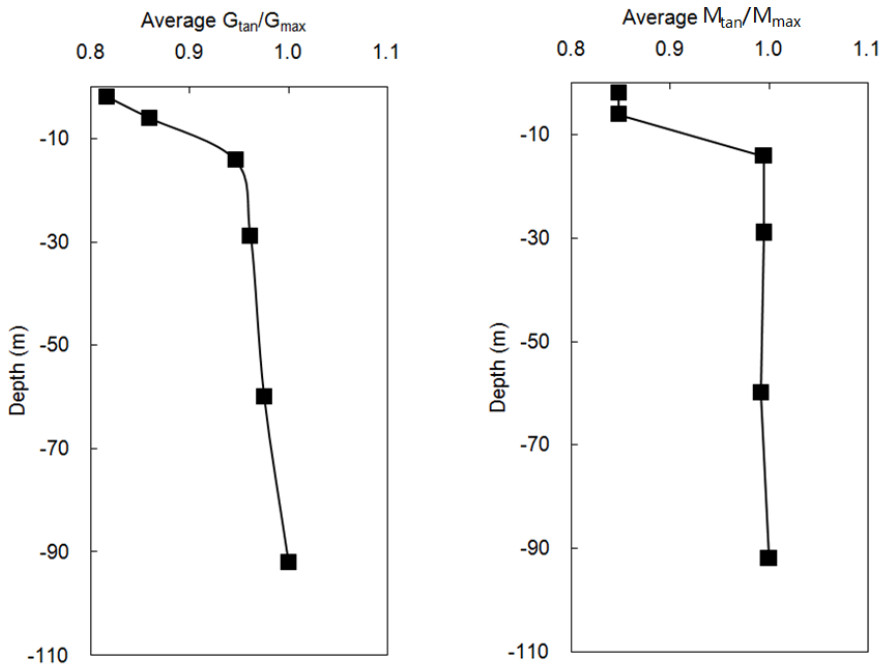

(a): Average shear modulus degradation (b): Average constrained modulus degradation

Figure 12: Average modulus degradation ratio variation

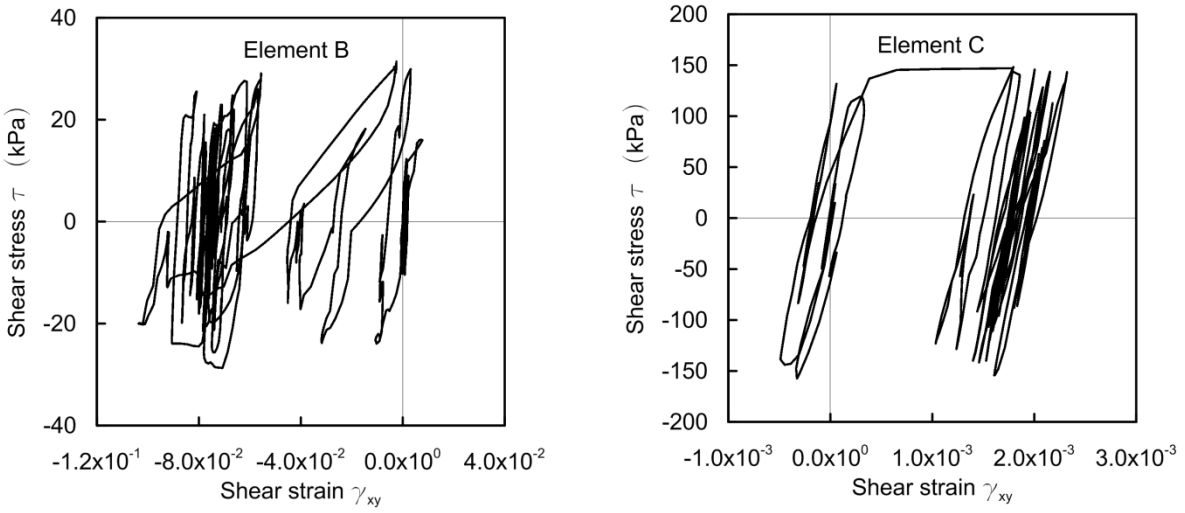

(a): Shear stress-strain response in EW direction

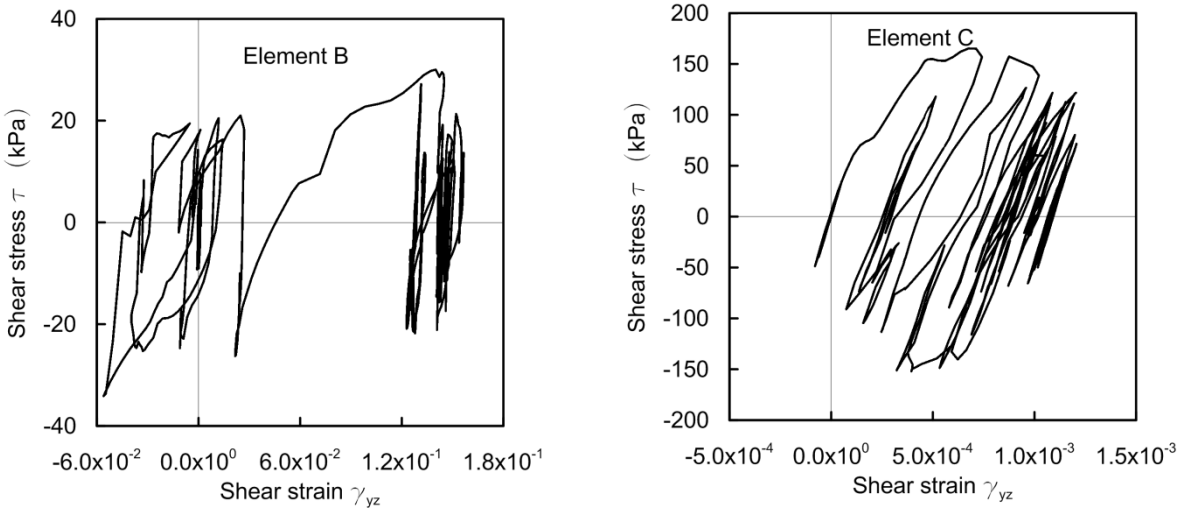

(b): Shear stress-strain response in NS direction

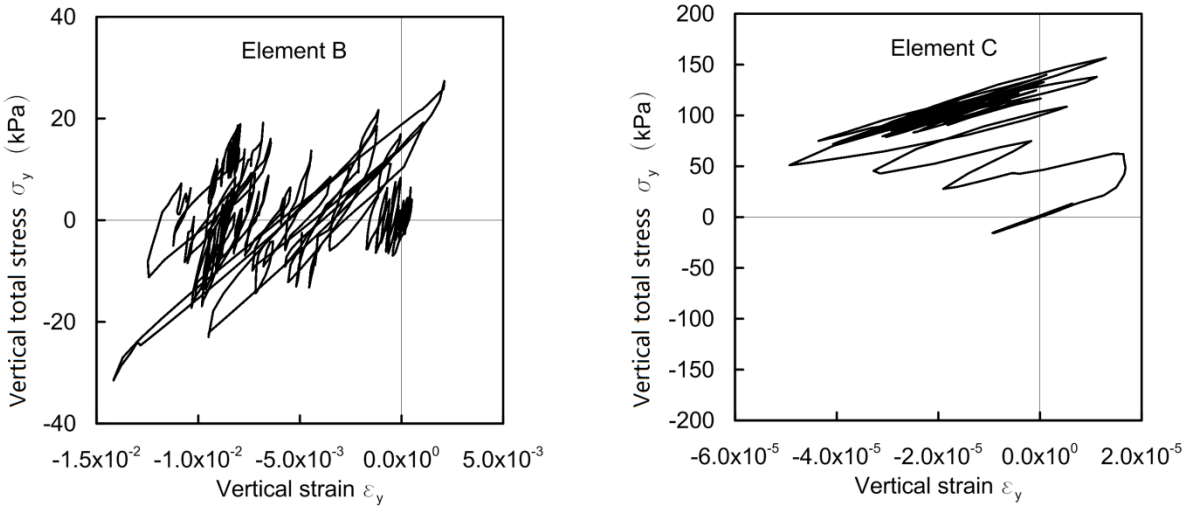

(c): Vertical stress-strain response in UD direction

Figure 13: Stress-strain response simulated by the nonlinear analysis

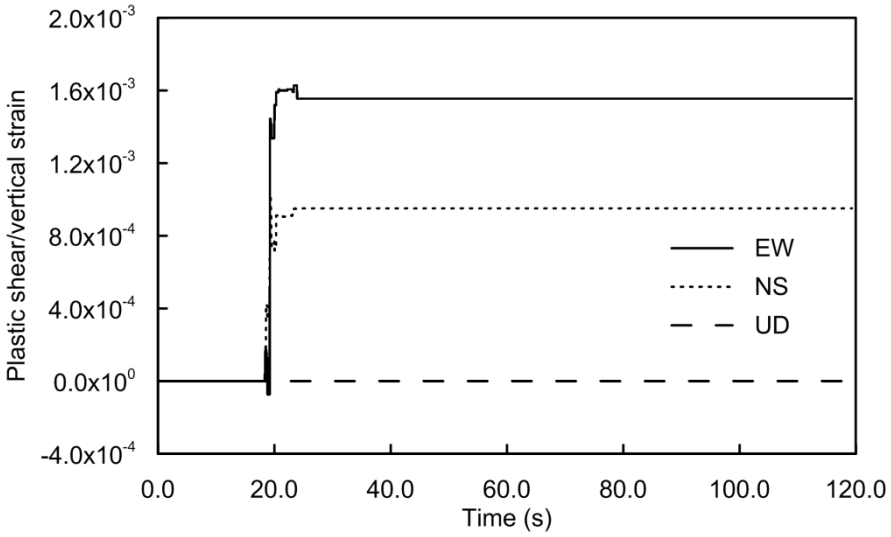

(a): 0-120s

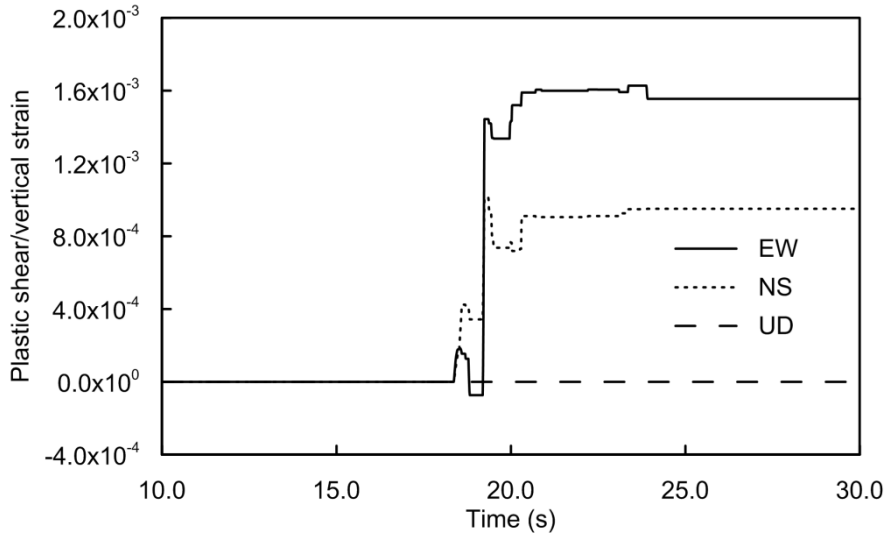

(b): 10-30s

Figure 14: Plastic strain time histories at element C simulated by the nonlinear analysis

6 Conclusions

In this paper, the multi-directional site response of the HINO site was investigated employing the 3-D dynamic HM formulation in ICFEP for two weak earthquake motions and the 2000 Western Tottori earthquake. The computed results were compared with the monitored data from the KiK-net downhole array system. The paper discussed the challenges that 3-D modelling poses to the calibration of a cyclic nonlinear model, giving particular emphasis to the independent simulation of shear and volumetric deformation

mechanisms.

Firstly, the site response of the HINO site subjected to two weak motions was computed with a cyclic nonlinear model (i.e. the ICG3S model). The effects of the independent simulation of shear and compressional deformation mechanisms on predicting multi-directional site response are investigated by comparing the predictions employing two versions of the ICG3S model, one that adopts the same degradation for shear and bulk moduli and the other one that independently simulates these two deformation mechanisms. The results show that the multi-directional site response subjected to the two weak motions is reasonably well simulated by the FE analysis with the independent simulation of shear and volumetric response, when compared with the monitored response. This version of the model is able to accurately predict both the horizontal and vertical site response simultaneously. Furthermore, the agreement with the recorded response indicates that the model is adequate to simulate realistically the material damping at very small strain levels.

In addition, the 3-D site response of the HINO site subjected to the 2000 Western Tottori earthquake was simulated employing the same cyclic nonlinear models. Overall, by employing the independent simulation of shear and volumetric deformation mechanisms, a good agreement was observed between the numerical results and the monitored site response, both in terms of acceleration time histories and response amplification spectra in the three directions. Once more, the model showed superior performance in terms of more realistic simulation of material damping at different concerned strain levels and independent simulation of stiffness degradation and material damping related to the shear and compressional responses. This highlights the significance of this numerical feature of the constitutive modelling on improving the numerical prediction of multi-directional site response. However, different calibrations were required for the earthquakes of different magnitudes, to achieve respective optimum calibration in the corresponding concerned strain ranges. This required an initial estimation of the seismically induced strains. Furthermore, soil nonlinearity was observed for all three directions, but this was more significant in the soil layer above the water table due to the smaller soil constrained modulus. The site response analysis predicted different deformation levels in the horizontal and vertical directions; the deformations were found to be in the medium to large strain range (i.e. $>10^{-1}$ %) and in the very small strain range ($<10^{-3}$ %) respectively as defined by Vucetic (1994) [37]. This highlighted the importance

of independent optimum calibration for the material damping related to the shear and compressional response at the respective relevant strain levels.

7 References

[1] Amorosi, A., Boldini, D. and Elia, G. (2010). Parametric study on seismic ground response by finite element modelling. *Computers and Geotechnics*, 37: 515-528.

[2] Amorosi, A., Boldini, D. and di Lernia A. (2016). Seismic ground response at Lotung: Hysteretic elasto-plastic-based 3D analyses, *Soil Dynamics and Earthquake Engineering*, 85:44-61.

[3] Anantanavanich, T., Pestana, J. and Carlton, B. (2012). Multidirectional site response analysis of submarine slopes using the constitutive model MSimpleDSS. Proceeding of the 15th World Conference on Earthquake Engineering, Lisbon, Portugal.

[4] Beresnev, I. A., Nightengale, A. M. and Silva, W. J. (2002). Properties of vertical ground motions. *Bulletin of the Seismological Society of America*, 92(8): 3152-3164.

[5] Borja, R. I., Chao, H. Y., Montans, F. J. and Lin, C. H. (1999). Nonlinear ground response at Lotung LSST site. *Journal of Geotechnical and Geoenvironmental Engineering*, 125(3): 187-197.

[6] Bowles, J. E. (1997). *Foundation analysis and design, 5th edition*. Peoria, Illinois: McGraw-Hill.

[7] Bradley, B. A. (2011). Near-source strong ground motions observed in the 22 February 2011 Christchurch earthquake. *Seismological Research Letters*, 82(6): 853-865.

[8] Chung, J. and Hulbert, G. M. (1993). A time integration algorithm for structural dynamics with improved numerical dissipation: the generalized-α method. *Journal of Applied Mechanics*, 60(2): 371-375.

[9] Darendeli, M. B. (2001). *Development of a new family of normalised modulus reduction and material damping curves*. PhD thesis, University of Texas at Austin.

[10] Domenico, P. A. and Schwartz, F. W. (1990). *Physical and Chemical Hydrogeology*. New York: John Wiley & Sons.

[11] Han, B. (2014). *Hydro-mechanical coupling in numerical analysis of geotechnical structures under multi-directional seismic loading*. PhD thesis, Imperial College London.

[12] Han, B., Zdravkovic, L. and Kontoe, S. (2015a). Stability investigation of the Generalised-a time integration method for dynamic coupled consolidation analysis. *Computers and Geotechnics*, 64: 83-95.

[13] Han B., Yang Z., Zdravković L. and Kontoe S. (2015). Non-linearity of gravelly soils under seismic compressional deformation based on KiK-net downhole array observations. *Geotechnique Letters*, 5(4): 287-293.

[14] Higashi, S. and Abe, S. (2002). Estimation of bedrock motions at KiK-net Hino site during the 2000

Tottori-ken Seibu earthquake based on the results of seismic reflection survey. The Proceedings of *the 11th Japan Earthquake Engineering Symposium (2002)*, Japan, 11: 461-464.

[15] Imazu, M. and Fukutake, K. (1986). Dynamic shear modulus and damping of gravel materials. The Proceedings of *the 21st Annual Meeting of JSSMFE*, Japan, 10: 509-512.

[16] Izutani, Y. (2004). Nonlinear response of surface layers at KiK-net stations in Japan. The Proceedings of *13th World Conference on Earthquake Engineering*, Vancouver, B.C., Canada, Paper No. 2690.

[17] Kaklamanos, J., Bradley, B. A., Thompson, E. M. and Baise, L. G. (2013). Critical parameters affecting bias and variability in site-response analyses using KiK-net downhole array data. *Bulletin of the Seismological Society of America*, 103(3): 1733-1749.

[18] Kondner, R. L. and Zelasko, J. S. (1963). A hyperbolic stress-strain formulation for sands. The Proceedings of *the 2nd Pan American Conference on Soil Mechanics and Foundations Engineering*, Brazil, 1: 289-324.

[19] Kontoe, S. (2006) *Development of time integration schemes and advanced boundary conditions for dynamic geotechnical analysis*. PhD thesis, Imperial College London, London, UK.

[20] Kontoe, S., Zdravkovic L. and Potts D. M. (2008). An assessment of time integration schemes for dynamic geotechnical problems, *Computers and Geotechnics*, 35: 253-264.

[21] Kontoe S., Zdravkovic L., Potts D.M. and Menkiti C.O. (2011). On the relative merits of simple and advanced constitutive models in dynamic analysis of tunnels. *Geotechnique*, 61: 815-829.

[22] LeBlanc, M. T., Stokoe, K. H., Branco, A. G. and Lee, R. C. (2012). Field determination of linear and nonlinear constrained moduli of soils using large mobile shakers. The Proceedings of *the 15th World Conference on Earthquake Engineering*, Lisbon, Portugal.

[23] Lee, C. P., Tsai, Y. B. and Wen, K. L. (2006). Analysis of nonlinear site response using the LSST downhole accelerometer array data. *Soil Dynamics and Earthquake Engineering*, 26: 435-460.

[24] Li, X. S., Shen, C. K. and Wang, Z. L. (1998). Fully coupled inelastic site response analysis for 1986 Lotung earthquake. *Journal of Geotechnical and Geoenvironmental Engineering*, 124: 560-573.

[25] Matasovic, N. and Vucetic, M. (1993). Cyclic characterization of liquefiable sands. *Journal of Geotechnical Engineering, ASCE*, 119(11):1805–22.

[26] Motamed, R., Stanton, K.V., Almufti, I., Ellison, K. and Willford, M. (2015). Effects of multi-directional shaking in nonlinear site response analysis: case study of 2007 Niigata-ken Chuetsu-oki Earthquake. Proceeding of the 6th International Conference in Earthquake Geotechnical Engineering, Christchurch, New Zealand.

[27] Muravskii, G. and Frydman, S. (1998). Site response analysis using a non-linear hysteretic model. *Soil Dynamics and Earthquake Engineering*, 17: 227-238.

[28] Papazoglou, A. J. and Elnashai, A. S. (1996). Analytical and field evidence of the damaging effect of vertical earthquake ground motion. *Earthquake Engineering and Structural Dynamics*, 25(2): 1109-1137.

[29] Phillips, C. and Hashash, Y. M. A. (2009). Damping formulation for nonlinear 1D site response analyses. *Soil Dynamics and Earthquake Engineering*, 29(7): 1143-1158.

[30] Potts, D. M. and Zdravkovic, L. (1999). *Finite element analysis in geotechnical engineering: Theory*. London: Thomas Telford.

[31] Puzrin, A. M. and Shiran, A. (2000). Effects of the constitutive relationship on seismic response of soils. Part I. Constitutive modeling of cyclic behavior of soils. *Soil Dynamics and Earthquake Engineering*, 19(5): 305-318.

[32] Sato, K., Kokusho, T., Matsumoto, M. and Yamada, E. (1996). Nonlinear seismic response and soil property during strong motion. *Soils and Foundations*, 36 (Special issue): 41-52.

[33] Taborda, D. M. G. (2011). *Development of constitutive models for application in soil dynamics*. PhD thesis, Imperial College London.

[34] Taborda, D. M. G. and Zdravkovic, L. (2012). Application of a Hill-Climbing technique to the formulation of a new cyclic nonlinear elastic constitutive model. *Computers and Geotechnics*, 43: 80-91.

[35] Taborda, D. M. G., Potts, D. M. and Zdravković L. (2016). On the assessment of energy dissipated through hysteresis in finite element analysis, *Computers and Geotechnics*, 71: 180-194.

[36] Tsaparli, V., Kontoe,S., Taborda,D.M.G. and Potts, D.M. (2016). Vertical ground motion and its effects on liquefaction resistance of fully saturated sand deposits. Proceedings of the Royal Society A, 472(2192):20160434.

[37] Vucetic, M. (1994). Cyclic threshold shear strains in soils. *Journal of Geotechnical Engineering*, 120(12): 2208-2228.

[38] Yang, J. and Sato, T. (2000). Interpretation of seismic vertical amplification observed at an array site. *Bulletin of the Seismological Society of America*, 90(2): 275-285.

[39] Yang, J. and Yan, X. R. (2009). Site response to multi-directional earthquake loading: A practical procedure. Soil Dynamics and Earthquake Engineering, 29(4): 710-721.

[40] Zienkiewicz, O. C., Chang, C. T. and BETTESS, P. (1980). Drained, undrained, consolidating and dynamic behaviour assumptions in soils. *Geotechnique*, 30(4): 385-395.